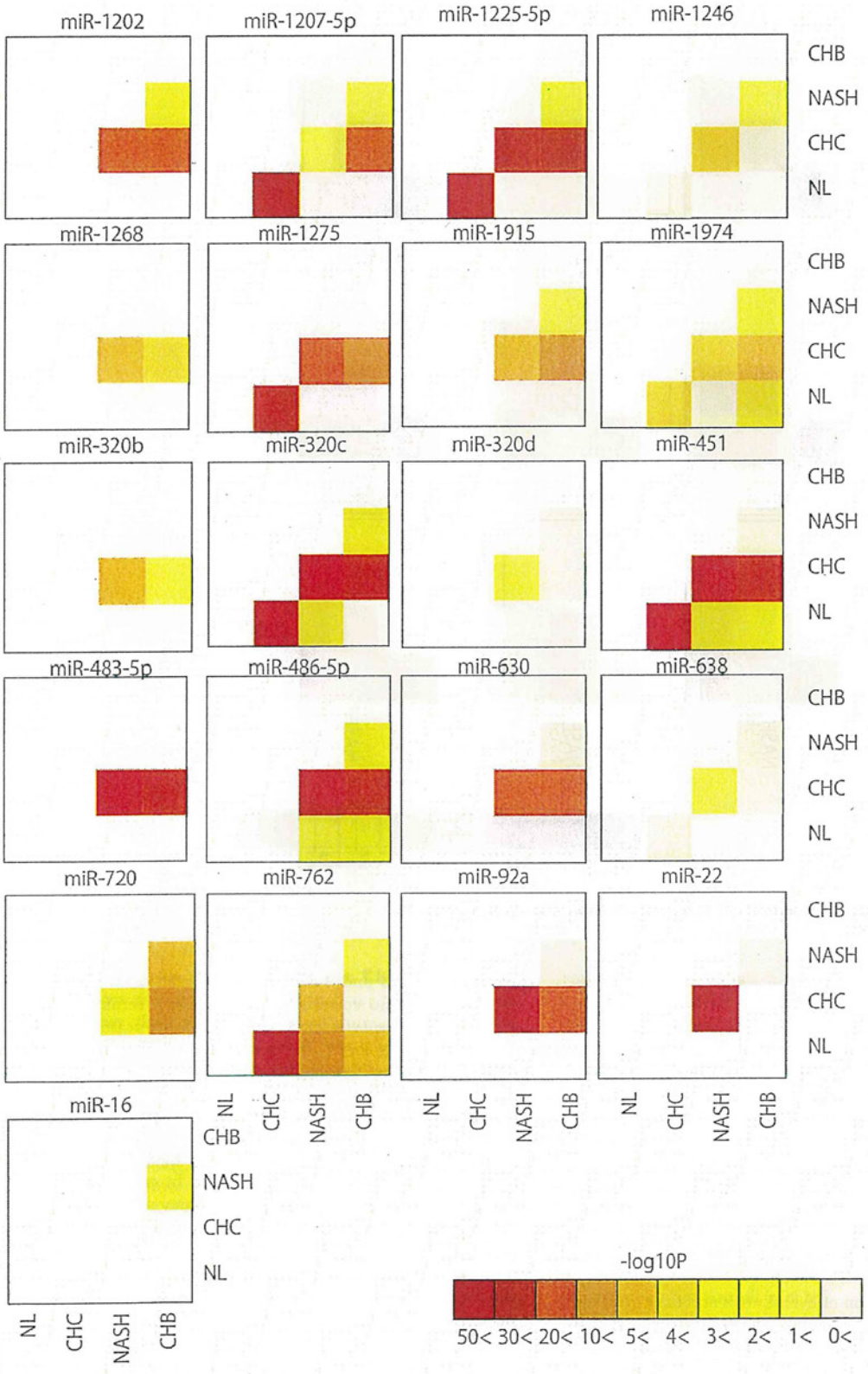

Figure 3. Pairwise heatmap of the miRNAs used for classifying two arbitrary groups. Pairwise heatmap showed the miRNAs and their p-value of two arbitrary groups.
doi:10.1371/journal.pone.0048366.g003

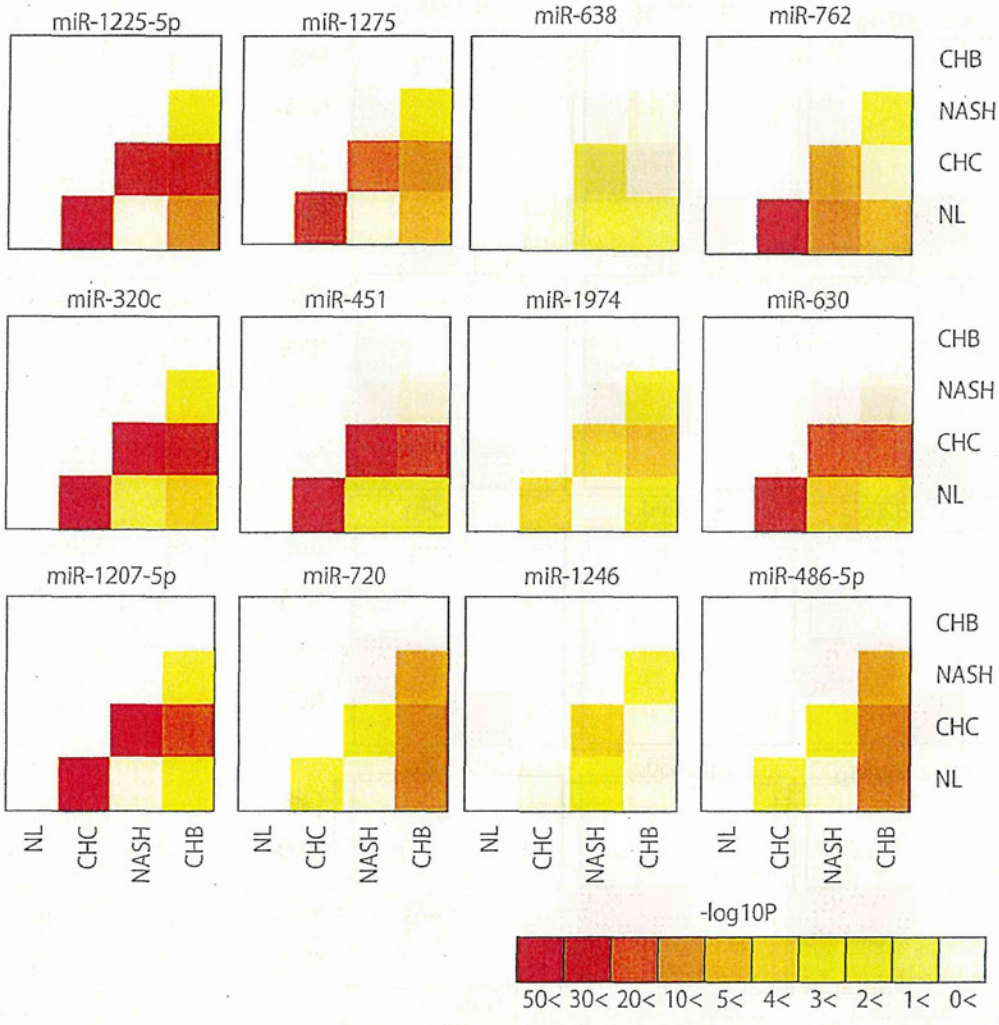

Figure 4. Pairwise heatmap of the miRNAs used for classifying among four groups.
doi:10.1371/journal.pone.0048366.g004

a significant positive correlation with the grade of liver inflammation, serum albumin value, or serum HCVRNA value. However, miR-122 expression did not significantly correlate with liver fibrosis stage. Moreover, there was no correlation between the expression level of miR-122 in liver tissue, and that in serum in the same 60 samples (**Fig. S14**). The expression pattern of only four miRNAs out of total liver tissue miRNAs correlated with the expression patterns of miRNA found in the serum (Table S4). Most serum miRNA had expression patterns that differed from those observed in hepatic tissue samples. Moreover, we observed differences in miRNAs expression between various tissues [32]. These differences were observed even in tissues taken from the same subject; at present we are unclear as to the reason for this phenomenon.

In regards to the progression of liver fibrosis and the expression pattern of miR-21, previous studies concur with our result that miR-21 expression level significantly decreased in response to the progression of liver fibrosis [20]. Taken together, this suggests that any miRNAs that may have been emitted from liver tissue cannot be detected in serum after hepatic cell injury.

The expression pattern of many miRNAs in serum positively correlated with serum ALT, albumin, and HCVRNA levels in this study (**Fig. 9, S13** and Table S3). This result contradicts prior assumptions that no correlation exists between serum miR-122 and HCVRNA serum levels [21]. Three likely reasons for this difference in results are: 1) the detection method used (real-time qPCR versus microarray), 2) the difference in the subjects' ages (the subjects in this study were older), and 3) the difference in the amount of miRNAs (multiple miRNAs vs. a single miRNA) used to identify the clinical parameters of the disease.

CHC and NL were classified with a high level of accuracy using the expression pattern of miRNA. In order to elucidate if the miRNA expression in CHC is common to other chronic liver diseases including CHB, we compared the miRNA expression pattern of CHC with those of NASH and CHB. The result of this analysis was that CHC could be clearly distinguished from both CHB and NASH. These results demonstrate that the varying forms of chronic liver disease have their own unique miRNA expression pattern. NASH is a histological diagnosis that rests on a combination of features and can only be confirmed by liver biopsy. Recently, NASH was diagnosed by first determining the existence of NAFLD from blood samples and then performing an ultrasound tomography. Finally, liver fibrosis stage was determined by Fibroscan

Table 1. Characteristics of subjects in this study of original samples and independent samples.

Original samples				
Characteristics	**CHC**	**CHB**	**NASH**	**NL**
Gender	F: 34/M: 30	F: 2/M: 2	F: 3/M: 9	F:11/M: 13
Age (years)	59.5±8.3	46.8±14.5	52.3±13.1	50.8±12.0
AST (IU/L)	50.1±29.8	83.3±53.7	46.2±16.0	N.D
ALT (IU/L)	57.6±40.6	167.8±170.3	74.5±34.9	N.D
WBC (x10^3/mm^3)	5.1±1.5	4.7±1.5	6.2±1.6	N.D
Platelet (x10^4/mm^3)	16.6±5.9	14.8±6.3	24.7±8.0	N.D
Total Bilirubin (mg/dl)	0.65±0.22	0.83±0.40	0.76±0.25	N.D
Weight (kg)	57.9±9.18	58.8±4.3	74.9±24.8	59.6±9.6
ALP (IU/L)	267.0±88.4	223.3±25.0	232.7±36.2	N.D
γGTP (IU/L)	46.9±42.3	77.3±82.2	58.4±20.9	N.D
Hemoglobin (g/dl)	13.8±1.2	14.5±0.59	14.7±1.6	N.D
Albumin (g/dl)	4.1±0.4	4.2±0.5	4.4±0.3	N.D
Independent samples				
Characteristics	**CHC**	**CHB**	**NASH**	
Gender	F: 18/M: 13	F: 10/M: 6	F: 6/M: 2	
Age (years)	59.5±8.3	46.8±14.5	54.8±12.7	
AST (IU/L)	50.1±29.8	83.3±53.7	80.9±50.0	
ALT (IU/L)	57.6±40.6	167.8±170.3	108.9±76.2	
WBC (x10^3/mm^3)	5.1±1.5	4.7±1.5	5.5±1.8	
Platelet (x10^4/mm^3)	16.6±5.9	14.8±6.3	19.3±7.6	
Total Bilirubin (mg/dl)	0.65±0.22	0.83±0.40	0.73±0.25	
Weight (kg)	57.9±9.18	58.8±4.3	66.4±9.9	
ALP (IU/L)	267.0±88.4	223.3±25.0	278.6±100.6	
γGTP (IU/L)	46.9±42.3	77.3±82.2	130.1±81.23	
Hemoglobin (g/dl)	13.8±1.2	14.5±0.59	13.6±1.4	
Albumin (g/dl)	4.1±0.4	4.2±0.5	3.8±0.3	

Abbreviations; CHC, chronic hepatitis C; CHB, chronic hepatitis B; NASH, non alcoholic steatohepatitis; NL, normal liver (healthy control); N.D, no data.
doi:10.1371/journal.pone.0048366.t001

(reviewed in [33]). However, when the results of these and other measures fail to yield a diagnosis then a pathology evaluation is necessary. Using "*in silico*" resampling to increase the reliability of our data, has led us to believe that NASH diagnosis may be possibly through blood examination.

We tested the reliability of our analysis in two ways and obtained reproducible results in both cases. First we enrolled an independent sample group, and second, we created virtual cohorts using in silico resampling to overcome our small sample size.

In this study we concluded that miRNA profiling is a promising alternative to diagnosing liver disease. This is based on our demonstration that the following evaluations could be performed using suitable miRNA expression profiles (1) determining the stage or grade of chronic liver disease, (2) ascertaining the clinical status of chronic liver diseases, and (3) distinguishing among various forms of chronic liver diseases. While these results suggest there is great potential and benefit of miRNA profiling, future studies in a larger population of CHC patients are warranted to fully elucidate the diagnostic potential of serum miRNA expression.

Materials and Methods

Patient Selection

A cohort of 64 CHC, 4 CHB, and 12 NASH patients who had undergone liver biopsy, as well as 24 healthy control subjects was enrolled. We also prepared independent samples consisting of 31 CHC, 12 CHB, and 8 NASH to validate our results. Patient characteristics are summarized in Table 1 and detailed clinical data is depicted in Table S5. The criteria for exclusion for CHC, CHB, and NASH were: co-infection with human immunodeficiency virus (HIV) types 1 and 2, decompensated liver disease, organ transplantation, immune suppression, autoimmune disorders, consumption of >20 g/day alcohol, and past history of intravenous drug abuse. Healthy controls were selected if they were not infected with HBV, HCV, nor HIV, had normal liver function tests, and had no history of liver disease.

All patients or their guardians provided written informed consent, and Ogaki Municipal Hospital and Kyoto University Graduate School and Faculty of Medicine's Ethics Committee approved all aspects of this study in accordance with the Helsinki Declaration.

Liver Histology and Blood Examination

A liver biopsy specimen was collected from each patient before anti-viral treatment. Histological grading and staging of CHC liver biopsy specimens were performed according to the Metavir classification system [34]. NASH was diagnosed histologically [35].

Serum HCV RNA was quantified before IFN treatment using Amplicor-HCV Monitor Assay (Roche Molecular Diagnostics Co., Tokyo, Japan), while serum HBV DNA was quantified before treatment using Amplicor HBV Monitor Assay (Roche). Pretreatment blood tests were conducted to determine each patient's level of aspartate aminotransferase (AST), alanine aminotransferase (ALT), total bilirubin, alkaline phosphatase, gamma-glutamyl transpeptidase, white blood cell (WBC), platelets, and hemoglobin.

Blood Sampling

Peripheral blood was collected from all subjects directly into serum tubes before anti-viral treatment. The tubes were centrifuged at 1,500 *g* for 10 min at 4°C, sera were aliquoted and additionally centrifuged at 2,000 *g* to completely remove any remaining cells. Sera were stored at −80°C until use.

RNA Preparation

Total RNA from 200 ul of serum was prepared using miRNeasy mini kit (Qiagen, Hilden Germany) according to the manufacturer's instruction. Exosome rich fractionated RNA was prepared using Exoquick (System Biosciences, CA, USA). Briefly, 900 ul of serum was mixed with 250 ul of Exoquick and incubated for 12 hr at 4°C. The tubes were centrifuged at 1500 g for 30 min at room temperature and then supernatant was discarded. The pellet was dissolved with 200 ul of PBS with vigorous vortex. RNA was extracted using miRNeasy mini kit (Qiagen).

Immunoblot Analysis and Exosome Preparation

The procedure for exosome preparation has been previously described [8]. SDS-PAGE gels, SuperSep Ace 5–20% (194–15021) (Wako, Osaka, Japan), were calibrated with Precision Plus Protein Standards (161–0375) (Bio-Rad), and anti-CD63 (1:200)

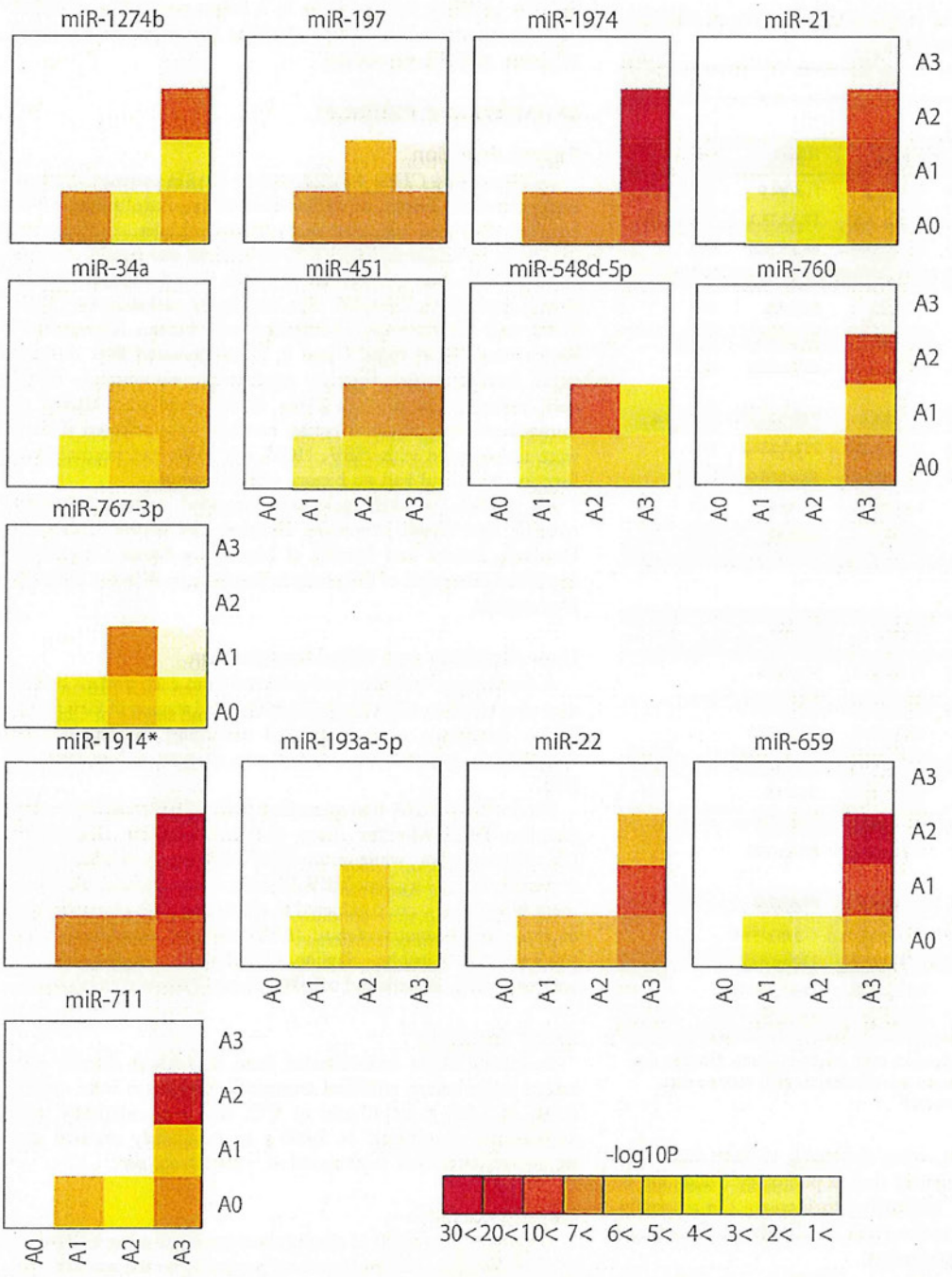

Figure 5. Significantly differentially expressed miRNAs according to liver inflammation grade. Pairwise heatmap showing the miRNAs and p-value of two arbitrary grades.
doi:10.1371/journal.pone.0048366.g005

was used as primary antibodies. The dilution ratio of each antibody is indicated in parentheses. Two secondary antibodies (peroxidase-labeled anti-mouse and anti-rabbit antibodies) were used at a dilution of 1:5000. Bound antibodies were visualized by chemiluminescence using the ImmunoStar LD (Wako) and luminescent images were analyzed by a LuminoImager (LAS-3000; Fuji Film, Inc.). Only gels for CD63 (BD, NJ, USA) detection were run under non-reducing conditions. To exclude the albumin and IgG in serum, Albumin & IgG Depletion SpinTrap kit was used (GE health care, WI, USA). After aliquots isolation, exosome-contained fraction was isolated by Exoquick according to standard instructions.

miRNA Microarray

To detect serum miRNA, 60 ng of RNA was labeled and hybridized using the Human microRNA Microarray Kit (Rel

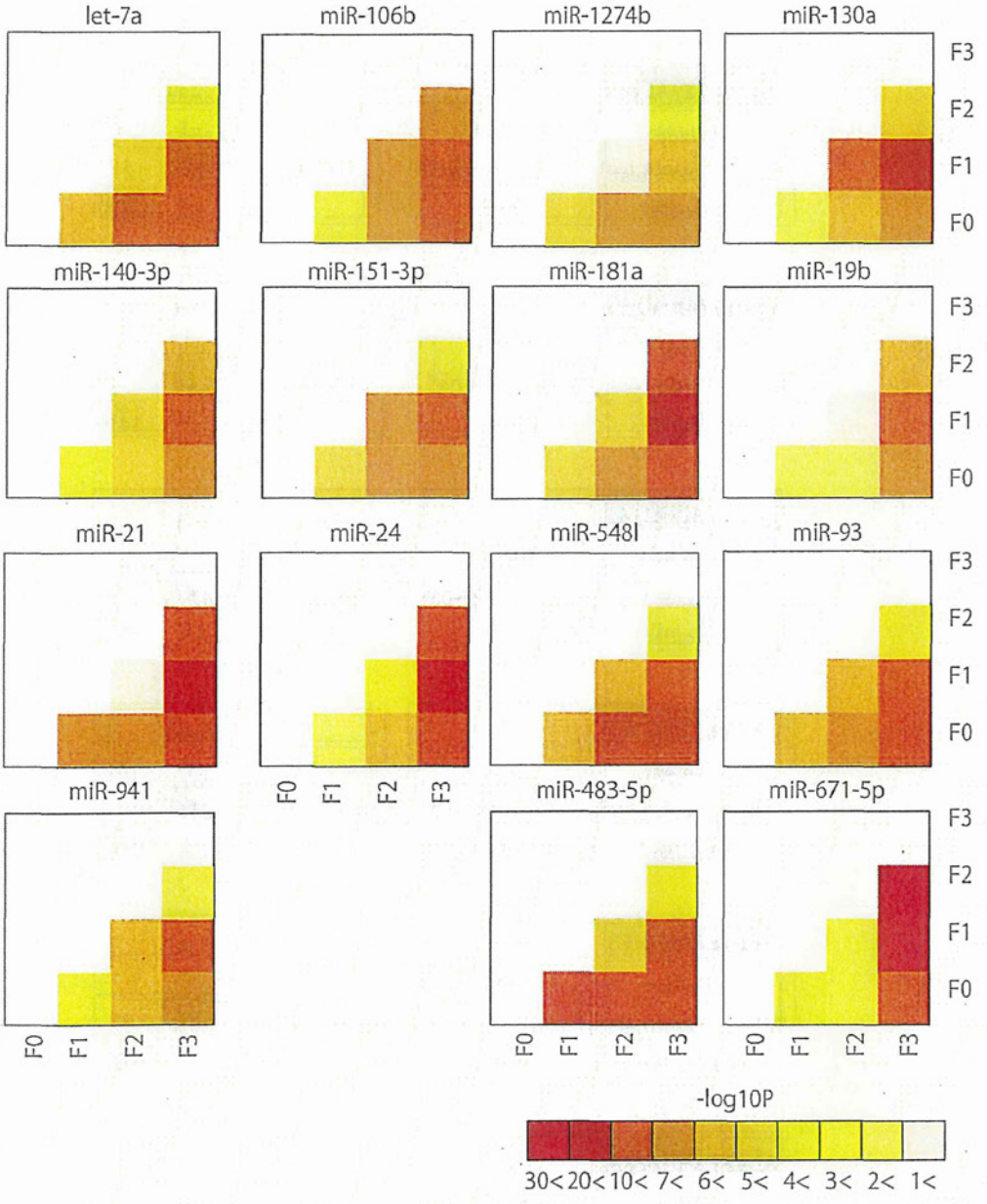

Figure 6. Significantly differentially expressed miRNA according to liver fibrotic stage. Pairwise heatmap showing the miRNAs and p-value of two arbitrary stages.
doi:10.1371/journal.pone.0048366.g006

14.0) (Agilent Technologies, CA, USA) according to the manufacturer's protocol (protocol for use with Agilent microRNA microarrays Version 1.0). Hybridization signals were detected with a DNA microarray scanner G2505B (Agilent Technologies) and the scanned images were analyzed using Agilent feature extraction software (v9.5.3.1). We used raw data (gProcessedSignal) and normalized each expression so as to have zero mean and unit sample variance. The data presented in this manuscript have been deposited in NCBI's Gene Expression Omnibus and are accessible through GEO Series access number GSE33857: http://www.ncbi.nlm.nih.gov/geo/query/acc.cgi?acc = GSE33857.

Real-time qPCR for Human miRNA

To detect miRNA expression level by real-time qPCR, TaqMan® microRNA assay (Applied Biosystems) was used to quantify the relative expression levels of miR-1207-5p (assay ID. 241060), miR-134 (assay ID. 000459), miR-1183 (assay ID. 002841), and miR-1249 (assay ID. 002868). The expression level of miR-16 (assay ID. 000391) was also measured and used as an internal control. cDNA was synthesized using the Taqman miRNA RT Kit (Applied Biosystems). RNA (2 ng/ml) in 5 ml of nuclease free water was added to 3 ml of 5 × RT primer, 10×1.5 µl of reverse transcriptase buffer, 0.15 µl of 100 mM dNTP, 0.19 µl of RNase inhibitor, 4.16 µl of nuclease free water, and 50 U of reverse transcriptase in a total volume of 15 µl. The reaction was performed for 30 min at 16°C, 30 min at 42°C, and 5 min at 85°C.

A

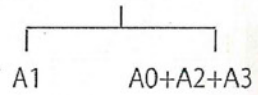

A1 vs A0+A2+A3	
accuracy	71.88%
Fisher's exact test	p-value: 4.07E-04
odds ratio	7.08

		result	
		F	T
prediction	F	22	12
	T	6	24

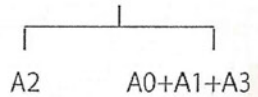

A2 vs A0+A1+A3	
accuracy	75.00%
Fisher's exact test	p-value:2.26E-04
odds ratio	9.50

		result	
		F	T
prediction	F	34	4
	T	12	14

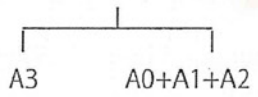

A3 vs A0+A1+A2	
accuracy	82.81%
Fisher's exact test	p-value: 2.30E-03
odds ratio	11.08

		result	
		F	T
prediction	F	47	3
	T	8	6

B

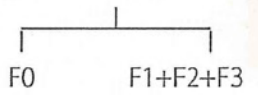

F0 vs F1+F2+F3	
accuracy	87.50%
Fisher's exact test	p-value: 4.95E-02
odds ratio	14.25

		result	
		F	T
prediction	F	54	1
	T	7	2

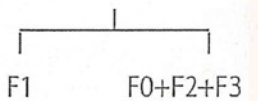

F1 vs F0+F2+F3	
accuracy	64.62%
Fisher's exact test	p-value: 2.73E-02
odds ratio	3.16

		result	
		F	T
prediction	F	21	13
	T	10	20

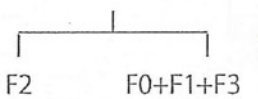

F2 vs F0+F1+F3	
accuracy	70.31%
Fisher's exact test	p-value: 3.24E-03
odds ratio	6.39

		result	
		F	T
prediction	F	33	4
	T	15	12

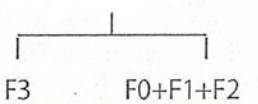

F3 vs F0+F1+F2	
accuracy	73.44%
Fisher's exact test	p-value: 1.35E-02
odds ratio	5.80

		result	
		F	T
prediction	F	39	4
	T	13	8

Figure 7. Determining liver inflammation grade and fibrotic stage using miRNA expression pattern in LOOCV analysis. A. In order to diagnose the grade of liver inflammation, A0 was identified first. Next A1, A2, and A3 were identified in a similar manner as A0. For each, the accuracy rate, P value, and the odds ratio are shown. B. For liver fibrosis stage, F0 was first diagnosed following which the other stages F1, F2, and F3 were diagnosed in a similar manner. For each group the accuracy rate, P value, and the odds ratio are shown.
doi:10.1371/journal.pone.0048366.g007

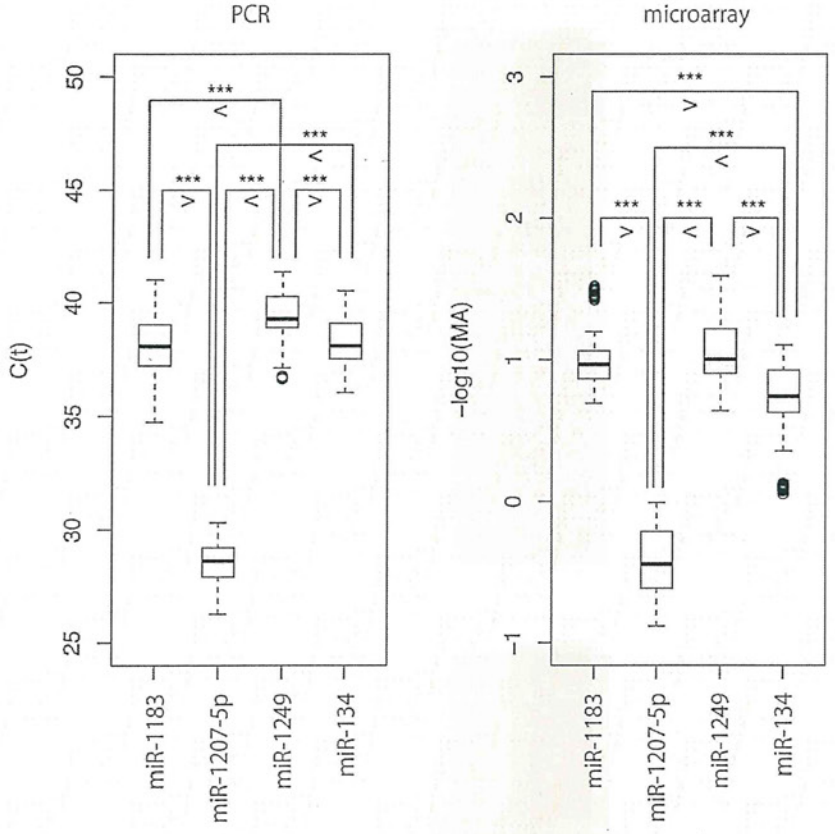

Figure 8. Real-time qPCR validation of microarray analysis. The microarray expression analysis result of four miRNAs was reproduced in real-time PCR analysis. The pairs with p<0.001 are marked by "***".
doi:10.1371/journal.pone.0048366.g008

All reactions were run in triplicate. Chromo 4 detector (Bio-rad) was used to detect miRNA expression. To allow for the validation of microarray results with C(t) obtained by qPCR, raw gene expressions were transformed into logarithmic values. P-values were computed via one-sided t test. No averages over probes were taken for the microarray. The above procedures were also done with various packages/functions implemented in R (http://www.r-project.org/).

Statistical Analysis

For symptoms having discrete values, grade pairs were compared with Wilcoxon rank sum test (one-sided); otherwise, P-values were computed from correlation coefficients. In both cases, false discovery rate (FDR) of less then 0.05 computed from the P-value was regarded as significant. Benjamini and Hochberg criterion was used for FDR estimation. All p-values shown are significant even though they are raw numbers. No average over probes was taken before correlation analyses.

The Canonical Correlation Coefficients for miRNA Expression and Clinical Parameters

The canonical correlation coefficients were computed for ALT-miRNA, albumin-miRNA, and HCVRNA-miRNA correlations, using up to 12 miRNA with larger correlation coefficients (see Supporting Information).

Classification Analyses for Liver Fibrosis/inflammation

P-values were computed via one-sided t test using the raw expression values of each miRNA from the samples of CHC and healthy controls. The logarithm of obtained P-values was then transformed into principal components scores via principal components analysis. Following this, grades were discriminated by linear discriminant analysis of CHC ages and the optimal number of principal components.

Selection of miRNAs Required to Diagnose Several Liver Diseases

For specific pairs consisting of one liver disease and a healthy control, their normalized miRNAs expression was transformed into principal components scores via principal components analysis. miRNAs having the larger first and second principal component scores were selected. Following this, the principal component scores of each sample was computed based solely on the selected miRNA expressions. Liver diseases were classified using the optimal number of these principal component scores.

In order to compensate for the relative small number of NASH and CHB patients, we performed "*in silico*" patients resampling analysis of the microarray data (see Supporting Information). All the above procedures were done with various packages/functions implemented in R.

"*In silico*" Resampling

"*In silico*" resampling is a tool often used to overcome the limitation of a small sample size. Using this technique, we combined the clinical traits of existing patients and created various virtual samples. Using these virtual cohorts, we were then able to increase the sample size (see Supporting information).

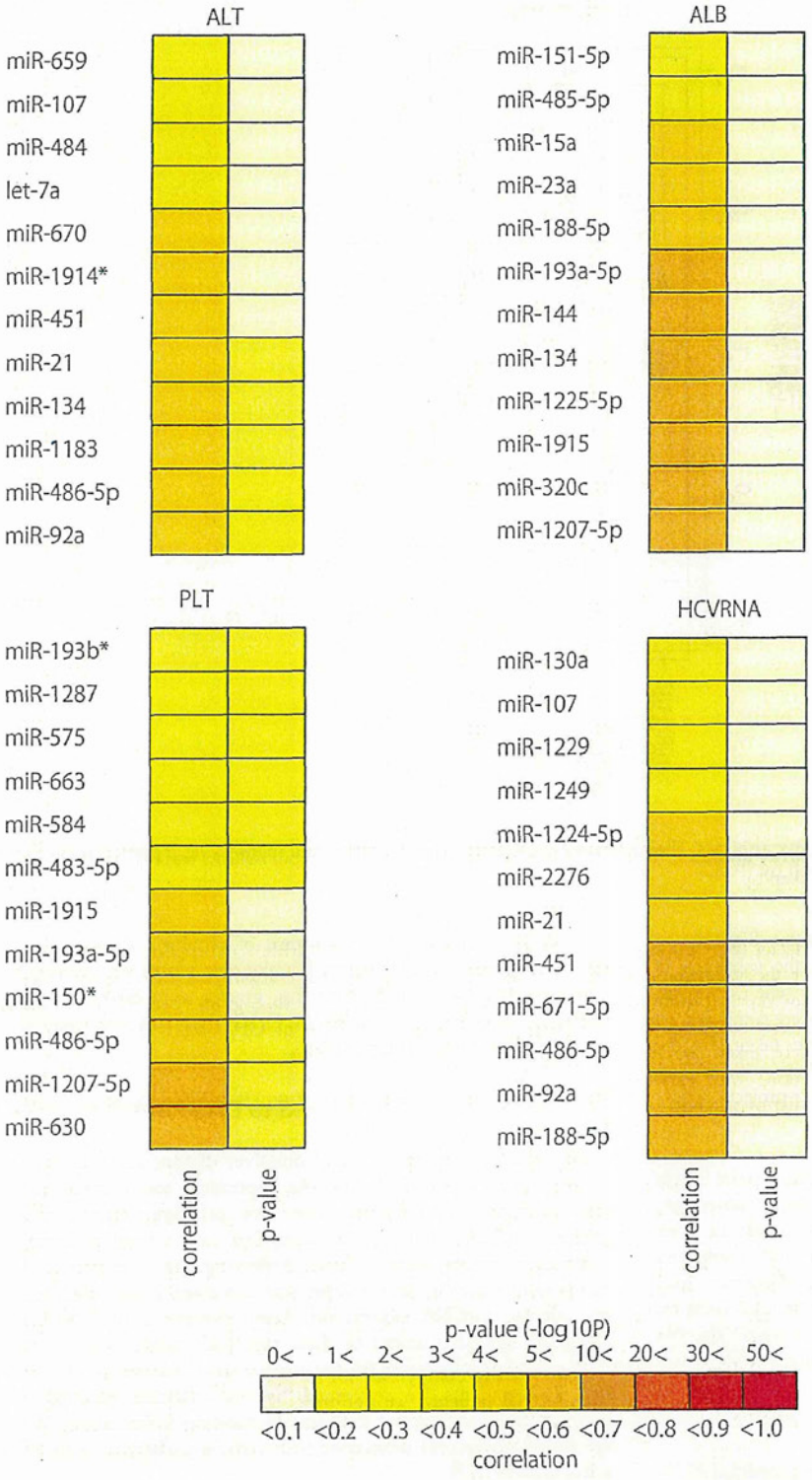

Figure 9. The list of miRNAs used to obtain the maximum correlation coefficient between miRNA expression level, and clinical characteristics. Pairwise heatmap showing miRNAs and their correlation coefficient and p-values.
doi:10.1371/journal.pone.0048366.g009

In order to validate the *"in silico"* resampling results, we prepared another sample set and once again performed *"in silico"* resampling using the microarray data from 99 CHC liver tissue samples [36]. The results proved that "*in silico*" resampling can accurately reproduce an entire population using only a small number of existing samples (see Supporting Information).

Reproducibility Test of Microarray Data

Data were analyzed using the GeneSpring GX10.0.2 (Agilent). Quality control (QC) was applied according to the manufacturer's instructions, and all data were approved by GeneSpring. Following Agilent recommendations, no inter-array normalization was applied because the similarity in miRNA expression among sample arrays was unknown [37]. Scatter plots and Pearson's pairwise correlations were performed with GeneSpring.

Supporting Information

Figure S1 Expression patterns of miRNAs used for discriminating among CHC, NL, CHB, and NASH. Classifying CHC, NL, CHB, and NASH using LOOCV. Distinguishing between two arbitrary groups using LOOCV.
(TIF)

Figure S2 Expression patterns of miRNAs used to discriminate among CHC, CHB, NASH, and NL "in silico" resampling for disease discriminant studies reflected by BMI. A. Box plots of expression pattern of the miRNAs used to discriminate among CHC, CHB, NASH, and NL. B. Discriminating among four groups using LOOCV. Accuracy is 95.25%. C. Two dimensional embedding of CHC, CHB, NASH, and NL by the first and second principle component scores computed with 12 selected miRNAs
(TIF)

Figure S3 The same as Fig.3 for CHC and CHB. A. Box plot of 19 miRNAs used for the discrimination. B. Classification between CHC and CHB. Accuracy is 100%. C. The two dimensional embedding of CHB and CHC by the first and second principal component scores computed with19 selected miRNAs.
(TIF)

Figure S4 The same as Fig.S3 for CHC and NASH. A. Box plots of 20 miRNAs used for the discrimination. B. Classification between CHC and NASH. Accuracy is 100%. C. Two dimensional embedding of CHC and NASH by the first and second principal component scores computed with 19 selected miRNAs
(TIF)

Figure S5 The same as Fig.S3 for CHC and NL. A. Box plots of 9 miRNAs used for the discrimination. B. Classification between CHC and NL. Accuracy is 100%. C. Two dimensional embedding of CHC and NL by the first and second principal component scores computed with 9 selected miRNAs
(TIF)

Figure S6 The same as Fig.S3 for CHB and NL. A. Box plots of 4 miRNAs used for the discrimination. B. Classification between CHB and NL. Accuracy is 93.5%. C. Two dimensional embedding of CHB and NL by the first and second principal component scores computed with 4 selected miRNAs
(TIF)

Figure S7 The same as Fig.S3 for NASH and NL. A. Box plots of 5 miRNAs used for the discrimination. B. Distinguishing between NASH and NL with 84.0% accuracy. C. Two dimensional embedding of NASH and NL by the first and second principal component scores computed with 5 selected miRNAs
(TIF)

Figure S8 The same as Fig.S3 for CHB and NASH pair. A. Box plots of 17 miRNAs used for the discrimination. B. Distinguishing between CHB and NASH with 80.0% accuracy. C. Two dimensional embedding of CHB and NASH by the first and second principal component scores computed with 17 selected miRNAs
(TIF)

Figure S9 Classification of the independent sample using semi-supervised learning based on the labels in the original cohort. A. Classifying CHB and CHC. Accuracy is 74.47%. B. Classifying CHC and NASH. Accuracy is 87.18%. C. Classifying CHB and NASH. Accuracy is 79.19%.
(TIF)

Figure S10 miRNA expression pattern that correlated with the changes in clinical background. miRNAs that were differentially expressed according to the grade of liver inflammation
(TIF)

Figure S11 miRNA expression pattern that correlated with the changes in clinical background. miRNAs that were differentially expressed according to liver fibrosis stage
(TIF)

Figure S12 Real-time qPCR validation of microarray analysis "in silico" resampling for disease discrimination studies reflected by BMI. The result of microarray expression analysis of four miRNAs was reproduced using real-time PCR analysis. Pairs with $p<0.001$ are marked by "***".
(TIF)

Figure S13 The relationship between the expression levels of several miRNAs and serum ALT, albumin, HCVRNA, respectively. Horizontal axis shows the number of miRNAs used in the analysis. Vertical axis shows the correlation index and p-values.
(TIF)

Figure S14 Summary of the relationship between the expression level of miR-122 and several clinical features. A. Expression level of miR-122 positively correlated with an increase in liver inflammatory grade. Asterisk denotes significant differences of $p<0.05$. B. Expression level of miR-122 positively correlated with the serum level of albumin. C. Expression level of miR-122 positively correlated with the amount of serum HCVRNA. D. Expression level of miR-122 in exosome rich fraction did not significantly correlate with that in liver tissues.
(TIF)

Table S1 The list of miRNAs used for classifying arbitrary 2 groups and 4 groups, and their p-values.
(DOCX)

Table S2 Significantly differentially expressed miRNAs according liver inflammation grade and liver fibrotic stage.
(DOCX)

Table S3 The list of miRNAs used to obtain the maximum correlation coefficient between expression level of miRNAs, and clinical characteristics.
(DOCX)

Table S4 List of miRNAs with expression that corresponded in liver tissue and serum.
(DOCX)

Table S5 Clinical background of original samples and independent samples in detail.
(DOCX)

Table S6 Accuracy of LDA for "in silico" resampling.
(DOCX)

Supplemental Information
(DOCX)

Author Contributions

Conceived and designed the experiments: YM NK TO YT. Performed the experiments: YM HT TT YY NK. Analyzed the data: TT YT. Contributed reagents/materials/analysis tools: HT JT TK. Wrote the paper: YM NK TO.

References

1. Ambros V (2004) The functions of animal microRNAs. Nature 431: 350–355.
2. Murakami Y, Toyoda H, Tanaka M, Kuroda M, Harada Y, et al. (2011) The progression of liver fibrosis is related with overexpression of the miR-199 and 200 families. PLoS One 6: e16081.
3. Murakami Y, Yasuda T, Saigo K, Urashima T, Toyoda H, et al. (2006) Comprehensive analysis of microRNA expression patterns in hepatocellular carcinoma and non-tumorous tissues. Oncogene 25: 2537–2545.
4. Braconi C, Henry JC, Kogure T, Schmittgen T, Patel T (2011) The role of microRNAs in human liver cancers. Semin Oncol 38: 752–763.
5. Hsu SH, Wang B, Kota J, Yu J, Costinean S, et al. (2012) Essential metabolic, anti-inflammatory, and anti-tumorigenic functions of miR-122 in liver. J Clin Invest 122: 2871–2883.
6. Tsai WC, Hsu SD, Hsu CS, Lai TC, Chen SJ, et al. (2012) MicroRNA-122 plays a critical role in liver homeostasis and hepatocarcinogenesis. J Clin Invest 122: 2884–2897.
7. Valadi H, Ekstrom K, Bossios A, Sjostrand M, Lee JJ, et al. (2007) Exosome-mediated transfer of mRNAs and microRNAs is a novel mechanism of genetic exchange between cells. Nat Cell Biol 9: 654–659.
8. Kosaka N, Iguchi H, Yoshioka Y, Takeshita F, Matsuki Y, et al. (2010) Secretory mechanisms and intercellular transfer of microRNAs in living cells. J Biol Chem 285: 17442–17452.
9. Zhang Y, Liu D, Chen X, Li J, Li L, et al. (2010) Secreted monocytic miR-150 enhances targeted endothelial cell migration. Mol Cell 39: 133–144.
10. Pegtel DM, Cosmopoulos K, Thorley-Lawson DA, van Eijndhoven MA, Hopmans ES, et al. (2010) Functional delivery of viral miRNAs via exosomes. Proc Natl Acad Sci U S A 107: 6328–6333.
11. Kogure T, Lin WL, Yan IK, Braconi C, Patel T (2011) Intercellular nanovesicle-mediated microRNA transfer: a mechanism of environmental modulation of hepatocellular cancer cell growth. Hepatology 54: 1237–1248.
12. Thery C, Ostrowski M, Segura E (2009) Membrane vesicles as conveyors of immune responses. Nat Rev Immunol 9: 581–593.
13. Mittelbrunn M, Gutierrez-Vazquez C, Villarroya-Beltri C, Gonzalez S, Sanchez-Cabo F, et al. (2011) Unidirectional transfer of microRNA-loaded exosomes from T cells to antigen-presenting cells. Nat Commun 2: 282.
14. Meckes DG Jr, Shair KH, Marquitz AR, Kung CP, Edwards RH, et al. (2010) Human tumor virus utilizes exosomes for intercellular communication. Proc Natl Acad Sci U S A 107: 20370–20375.
15. Gould SJ, Booth AM, Hildreth JE (2003) The Trojan exosome hypothesis. Proc Natl Acad Sci U S A 100: 10592–10597.
16. Kosaka N, Iguchi H, Ochiya T (2010) Circulating microRNA in body fluid: a new potential biomarker for cancer diagnosis and prognosis. Cancer Sci 101: 2087–2092.
17. Mitchell PS, Parkin RK, Kroh EM, Fritz BR, Wyman SK, et al. (2008) Circulating microRNAs as stable blood-based markers for cancer detection. Proc Natl Acad Sci U S A 105: 10513–10518.
18. Chen X, Ba Y, Ma L, Cai X, Yin Y, et al. (2008) Characterization of microRNAs in serum: a novel class of biomarkers for diagnosis of cancer and other diseases. Cell Res 18: 997–1006.
19. Lawrie CH (2007) MicroRNAs and haematology: small molecules, big function. Br J Haematol 137: 503–512.
20. Cermelli S, Ruggieri A, Marrero JA, Ioannou GN, Beretta L (2011) Circulating microRNAs in patients with chronic hepatitis C and non-alcoholic fatty liver disease. PLoS One 6: e23937.
21. Bihrer V, Friedrich-Rust M, Kronenberger B, Forestier N, Haupenthal J, et al. (2011) Serum miR-122 as a biomarker of necroinflammation in patients with chronic hepatitis C virus infection. Am J Gastroenterol 106: 1663–1669.
22. Ji F, Yang B, Peng X, Ding H, You H, et al. (2011) Circulating microRNAs in hepatitis B virus-infected patients. J Viral Hepat 18: e242–251.
23. Starkey Lewis PJ, Dear J, Platt V, Simpson KJ, Craig DG, et al. (2011) Circulating microRNAs as potential markers of human drug-induced liver injury. Hepatology 54: 1767–1776.
24. Chapelle O, Scholkopf B, Zien A (2006) Semi-supervised learning. Cambridge, Mass.: MIT Press. x, 508 p. p.
25. Hunter MP, Ismail N, Zhang X, Aguda BD, Lee EJ, et al. (2008) Detection of microRNA expression in human peripheral blood microvesicles. PLoS One 3: e3694.
26. Marquez RT, Bandyopadhyay S, Wendlandt EB, Keck K, Hoffer BA, et al. (2010) Correlation between microRNA expression levels and clinical parameters associated with chronic hepatitis C viral infection in humans. Lab Invest 90: 1727–1736.
27. Mathivanan S, Ji H, Simpson RJ (2010) Exosomes: extracellular organelles important in intercellular communication. J Proteomics 73: 1907–1920.
28. Simons M, Raposo G (2009) Exosomes–vesicular carriers for intercellular communication. Curr Opin Cell Biol 21: 575–581.
29. Keller A, Leidinger P, Bauer A, Elsharawy A, Haas J, et al. (2011) Toward the blood-borne miRNome of human diseases. Nat Methods 8: 841–843.
30. Laterza OF, Lim L, Garrett-Engele PW, Vlasakova K, Muniappa N, et al. (2009) Plasma MicroRNAs as sensitive and specific biomarkers of tissue injury. Clin Chem 55: 1977–1983.
31. Nathwani RA, Pais S, Reynolds TB, Kaplowitz N (2005) Serum alanine aminotransferase in skeletal muscle diseases. Hepatology 41: 380–382.
32. Landgraf P, Rusu M, Sheridan R, Sewer A, Iovino N, et al. (2007) A mammalian microRNA expression atlas based on small RNA library sequencing. Cell 129: 1401–1414.
33. Dowman JK, Tomlinson JW, Newsome PN (2011) Systematic review: the diagnosis and staging of non-alcoholic fatty liver disease and non-alcoholic steatohepatitis. Aliment Pharmacol Ther 33: 525–540.
34. Bedossa P, Poynard T (1996) An algorithm for the grading of activity in chronic hepatitis C. The METAVIR Cooperative Study Group. Hepatology 24: 289–293.
35. Matteoni CA, Younossi ZM, Gramlich T, Boparai N, Liu YC, et al. (1999) Nonalcoholic fatty liver disease: a spectrum of clinical and pathological severity. Gastroenterology 116: 1413–1419.
36. Murakami Y, Tanaka M, Toyoda H, Hayashi K, Kuroda M, et al. (2010) Hepatic microRNA expression is associated with the response to interferon treatment of chronic hepatitis C. BMC Med Genomics 3: 48.
37. Zhang X, Chen J, Radcliffe T, Lebrun DP, Tron VA, et al. (2008) An array-based analysis of microRNA expression comparing matched frozen and formalin-fixed paraffin-embedded human tissue samples. J Mol Diagn 10: 513–519.

Chapter 17

In Vivo Imaging of Oligonucleotide Delivery

Fumitaka Takeshita, Ryou-u Takahashi, Jun Onodera, and Takahiro Ochiya

Abstract

RNA interference (RNAi) has rapidly become a powerful tool for drug-target discovery and therapeutics. Cancer is an important application for RNAi therapeutics, since abnormal gene regulation is thought to contribute to the pathogenesis and maintenance of the metastatic phenotype of cancer. Many oncogenic genes present enticing therapeutic target possibilities for RNAi. Small interfering RNA (siRNA) and microRNA (miRNA) are potent and specific examples of RNAi are able to silence tumor-related genes and multiple oncogenic pathways and appear to be a rational approach to inhibit tumor growth. In subsequent in vivo studies, an appropriate animal model must be developed for a better evaluation of gene-silencing effects on tumors. How to evaluate the effect of siRNA and miRNA in an in vivo therapeutic model is also important. Bioluminescence imaging is an optical imaging method that can evaluate RNAi in vivo.

Key words: siRNA, MicroRNA, Cancer, Delivery, Imaging, Luciferase, Oligonucleotides

1. Introduction

RNAi can effect posttranscriptional gene silencing. The introduction into an organism of double-stranded RNA (dsRNA) corresponding to a transcribed sequence results in degradation of the corresponding mRNA (1–6). With RNAi, dsRNA blocks gene expression in a sequence-specific manner. When introduced into cells, dsRNA is processed by the RNase III family nuclease Dicer into siRNA, 21-basepair dsRNA with two overhanging bases at each 3′ terminus. The double-stranded siRNA is passed to the RNA-induced silencing complex (RISC), an RNA–nuclease complex, which is activated as it unwinds the duplex and incorporates one of the antisense strands. The RISC then selectively degrades

Robert M. Hoffman (ed.), *In Vivo Cellular Imaging Using Fluorescent Proteins: Methods and Protocols*,
Methods in Molecular Biology, vol. 872, DOI 10.1007/978-1-61779-797-2_17,

RNA containing the sequence complementary to the incorporated antisense strand.

Antisense oligonucleotide drugs were used prior to the discovery of RNAi and several antisense molecules are currently in late-stage preclinical or clinical development (7). Although researchers continue to explore and develop antisense reagents for therapeutic use by morpholino oligomers, a fourth class of oligonucleotide-based compounds, consisting of siRNAs, has recently become widely used for gene knockdown in vitro and in vivo.

Another group of catalytically-active RNA molecules (ribozymes) has also been considered for therapeutic use. However, only a few ribozymes have turned out to be efficient compounds in clinical trials. RNAi is effective because siRNA is highly specific for the target gene, and the single-strand RNA molecule incorporated into the RISC is used to recognize multiple copies of the target RNA. Therefore, an extremely small amount of siRNA can generate reliable gene suppression, making toxicity less of a concern. Furthermore, effective antisense oligonucleotide sequences are determined empirically, resulting in uncertain efficacies.

MicroRNA (miRNA), an endogenously-expressed form of siRNA, approximately 22 nucleotides in length, also works for gene silencing. It is estimated that there are over 1,000 miRNAs in humans. It is believed that a single miRNA can regulate several hundred genes. Current understanding of the molecular mechanism of any disease, including cancer (8, 9), would be incomplete without factoring in the functional significance of miRNA. Misexpression of miRNAs has been observed in various types of cancers and is also associated with the clinical outcome of cancer patients. Consistently, miRNAs have been implicated in the regulation of various cellular processes that are often deregulated during tumor development and progression (10, 11), suggesting that these miRNAs might be targets for cancer therapy.

The most direct way for molecules to correct expression of altered genes and miRNAs is treatment by RNA oligonucleotides. For this purpose, an in vivo delivery system is a key issue. Here, we describe an in vivo imaging method of delivery of oligonucleotides such as siRNA and miRNA.

2. Materials

2.1. Cell Lines and Medium

1. PC-3M-luc cells (Xenogen Corp., Alameda, CA).
2. Cell culture medium: RPMI 1640 medium (Invitrogen Corp., Carlsbad, CA) supplemented with 10% heat-inactivated fetal bovine serum (Equitech-Bio, Kerrville, TX) and 0.2 mg/ml zeocin (Invitrogen Corp.).

2.2. Oligonucleotide Delivery Mixture

1. Oligonucleotide delivery system: atelocollagen (12–15) for local use AteloGene™ #1390 and systemic use AteloGene™ #1391 (Koken, Tokyo).
2. Oligonucleotides: 5–10 and 20–40 μM oligonucleotide solutions for local and systemic delivery in vivo.

2.3. In Vivo Imaging

1. For in vivo imaging with Renilla luciferase: ViviRen (5 mg/kg, Promega).
2. For in vivo imaging with firefly luciferase: D-luciferin (150 mg/kg, Xenogen).
3. Data analysis: LivingImage software (version 2.50, Xenogen) (16).

3. Methods

Recent progress in the optical imaging of cancers in animal models presents many potential advantages for recreating the disease process, disease detection, screening, diagnosis, drug development, and treatment evaluation. Fluorescence-based imaging (17–21) and bioluminescence-based imaging (12, 13, 22–29) are well developed and allow specific, highly-sensitive, and quantitative measurements of a wide range of tumor-related parameters in mice.

A major advantage of GFP-labeling is that imaging requires no preparative procedures and hence allows for direct visualization in living tissue. In contrast, luciferase imaging requires exogenous injection of luciferin substrate which can stress the animals. In addition, the intensity of the luciferase signal may sometimes be variable and unstable. Furthermore, RFP imaging is about 1,000 times stronger than that of luciferase in vivo. Therefore, for monitoring the tumor metastasis process at the single-cell level, fluorescence imaging may be the more practical method. In fact, fluorescence-based orthotopic metastatic models have been used to study mechanisms and drug discovery. Here, we have used the bioluminescence signal from the luciferase reporter gene in our metastasis model. Luciferase genes in our tumor cells can function stably over significant periods of time in tumors and in their metastases.

3.1. Preparation of Dual Luciferase Expressing Cells

1. For construction of 3′-UTR-Renilla luciferase plasmid and reporter assays, amplify the segment of 3′-UTR of the Bcl2 gene by PCR using genomic DNA from normal human prostate epithelial cells (PrEC, CT-2555, Lonza Walkersville, Inc., Walkersville, MD).
2. Insert the PCR product into a pGL4.75 [HRuc/CMV] vector (Promega, Madison, WI), using the XbaI site immediately

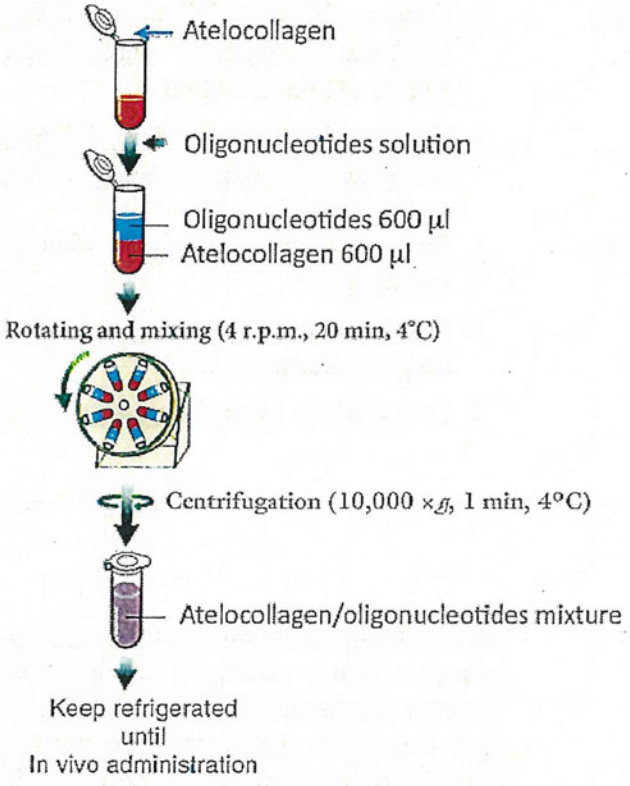

Fig. 1. Preparation of oligonucleotides delivery mixture. Gently add 600 µl of the oligonucleotide solution to 600 µl of the atelocollagen solution. Rotate the mixture solution for 20 min. Set the rotating speed at about 4 rpm when a 20-cm diameter holder is used. After mixing, centrifuge the tube for 1 min at 10,000 x *g* to deform the mixed solution.

downstream from the stop codon of Renilla luciferase (pGL4.75[HRuc/CMV]-Bcl2 3′UTR).

3. For reporter assays, transfect 2 µg pGL4.75[HRuc/CMV]-Bcl2 3′UTR using LipofectAMINE™ 2000 (Invitrogen Corp.) into PC-3M-luc cells.
4. Select stable transfectants in hygromycin (0.2 mg/ml; Invitrogen Corp.) using the Dual-luciferase assay-system (Promega). The intensity of Renilla luciferase is normalized by firefly luciferase. Clones expressing both luciferase genes are named PC-3M-luc/Rluc-Bcl2 3′UTR.

3.2. Oligonucleotides Delivery

1. Gently add 600 µl of the oligonucleotide solution to 600 µl atelocollagen solution.
2. Rotate the mixture solution for 20 min. Set the rotating speed at approximately 4 rpm when using a 20-cm diameter holder (see Note 1).
3. After mixing, centrifuge the tube for 1 min at 10,000×*g* to deform the mixed solution (see Note 2). The procedure is shown in Fig. 1.

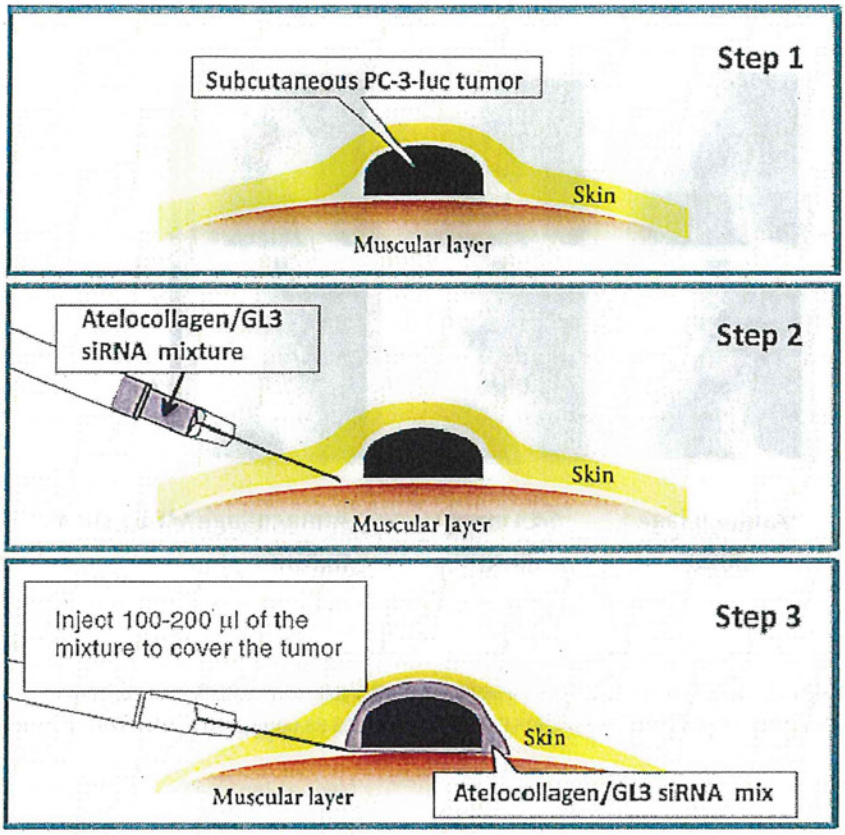

Fig. 2. Administration of the mixture to subcutaneous tumors. Step 1: PC-3-luc subcutaneous tumor; Step 2: insert a 26 G needle subcutaneously approximately 5 mm to the side of the tumor; Step 3: lay the needle parallel to the skin and insert it for 2–3 mm in the direction of the tumor, and then inject the mixture for 20–30 s. It is effective when the mixture is administered so as to cover the whole target site.

3.3. Imaging of Local Delivery of Oligonucleotides

1. Prepare 7- to 10-week-old male athymic nude mice (CLEA Japan, Shizuoka, Japan).
2. To generate a subcutaneous tumor model, the animals are injected with 1×10^6 PC-3-luc cells suspended in 100-ml sterile DPBS.
3. When a tumor develops to 5×5 mm a mixture of GL3 siRNA (specifically knock down firefly luciferase) and atelocollagen are prepared according to the described method.
4. Set the 18-G needle in the disposable syringe and slowly draw the atelocollagen/oligonucleotide mixture (see Note 3).
5. Replace the needle of the syringe with a 26-G injection needle and keep the syringe refrigerated until administration.
6. Insert the injection needle from approximately 5 mm to the side of the subcutaneous tumor with the cut face of the needle turned upward.
7. Lay the needle parallel to the skin and insert it 2–3 mm in the direction of the tumor, and then gently inject 200 µl of the mixture. The procedure is shown in Fig. 2 (see Note 4).

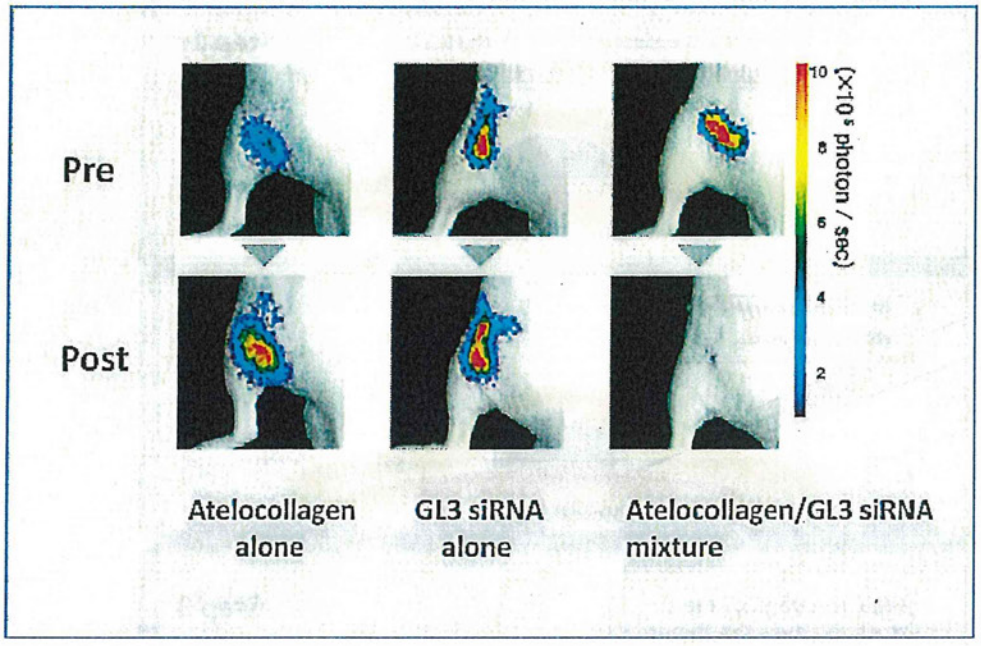

Fig. 3. In vivo imaging of local delivery of oligonucleotides. Firefly luciferase-expressing cells formed subcutaneous tumors. Atelocollagen/GL3 siRNA significantly inhibited the photon count of luciferase as compared to atelocollagen alone and GL3 siRNA alone.

8. 24–48 h after injection (see Note 5), the animals are subjected to bioimaging analysis. An example result is shown in Fig. 3.

3.4. Imaging of Systemic Delivery of Oligonucleotides

1. To generate an experimental metastasis model, the anesthetized animals are injected with 2×10^6 PC-3M-luc cells suspended in 100 ml sterile DPBS into the left heart ventricle (see Note 6).
2. When metastasis develops, a mixture of GL3 siRNA and atelocollagen is prepared according to the above method.
3. Anesthetize the animals, if necessary.
4. Set the 18-G needle in a disposable syringe and slowly draw the atelocollagen/oligonucleotide mixture. In a systemic injection, 100–200 µl of the mixture is used.
5. Replace the syringe needle with the 26-G injection needle and keep the syringe refrigerated until administration.
6. Disinfect the tail of the animal with ethanol.
7. Insert the needle into the vein at a position 1/4 from the tail end.
8. Confirm that the injection needle has entered the vessel and then slowly inject 100–200 µl of the mixture (see Note 7).
9. 24–48 h after injection, the animals are subjected to bioimaging analysis. An example result is shown in Fig. 4.

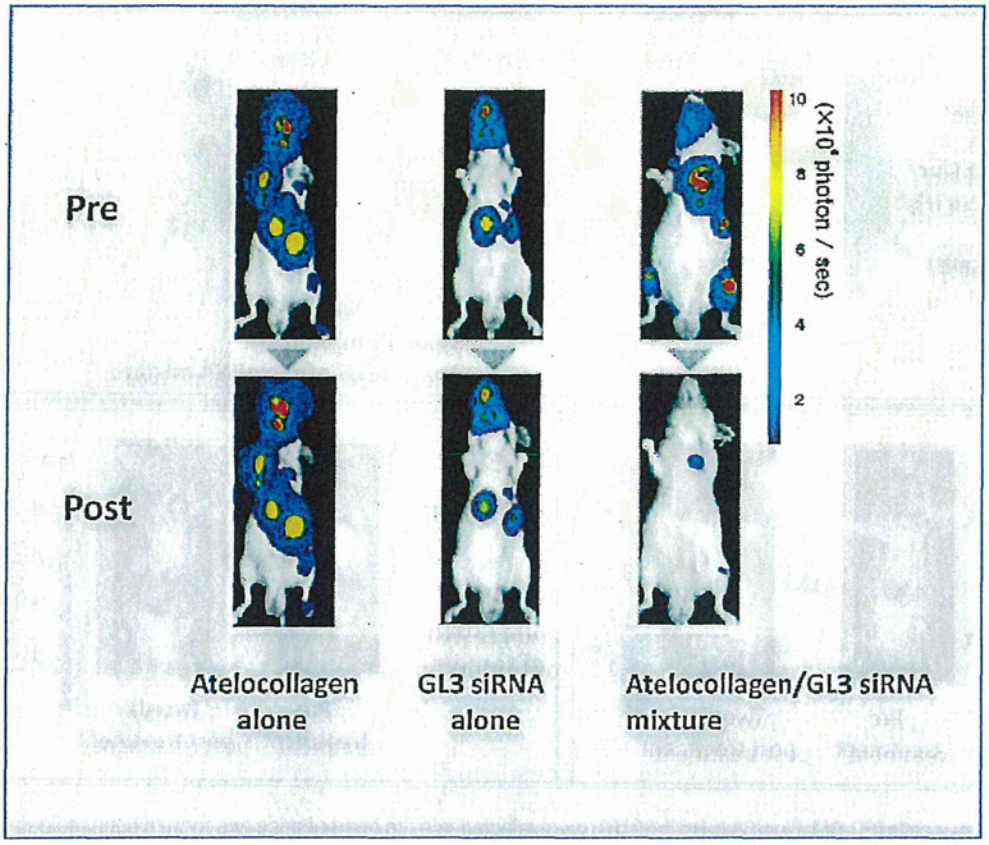

Fig. 4. Firefly-luciferase-expressing cells with formed bone metastasis in mice. Intra-cardiac administration of atelocollagen/GL3 siRNA significantly inhibited the photon count of luciferase as compared to atelocollagen alone and GL3 siRNA alone.

3.5. Dual Luciferase Imaging System for Delivery of Oligonucleotides

1. Seven- to ten-week-old male athymic nude mice (CLEA Japan, Shizuoka, Japan) are anesthetized by exposure to 3% isoflurane on day 0 and subsequent days.
2. On day 0 of the experiments, to generate an experimental metastasis model, the anesthetized animals are injected with 2×10^6 PC-3M-luc/Rluc-Bcl2 3′UTR cells, suspended in 100 ml sterile DPBS, into the left heart ventricle.
3. When metastasis develops, a mixture of miRNA16 and atelocollagen is prepared according to the described method.
4. For systemic injection of the atelocollagen/miRNA mixture, repeat steps 4–8 in Subheading 3.2.
5. For in vivo imaging, the mice are injected with ViviRen (5 mg/kg, Promega) by intravenous tail vein injection and imaged immediately to count the photons from the animal body.
6. After the bioluminescence from Renilla luciferase disappears, the mice are administered D-luciferin (150 mg/kg, Xenogen) by intraperitoneal injection.
7. Ten minutes later, photons from firefly luciferase are counted. An example result is shown in Fig. 5.

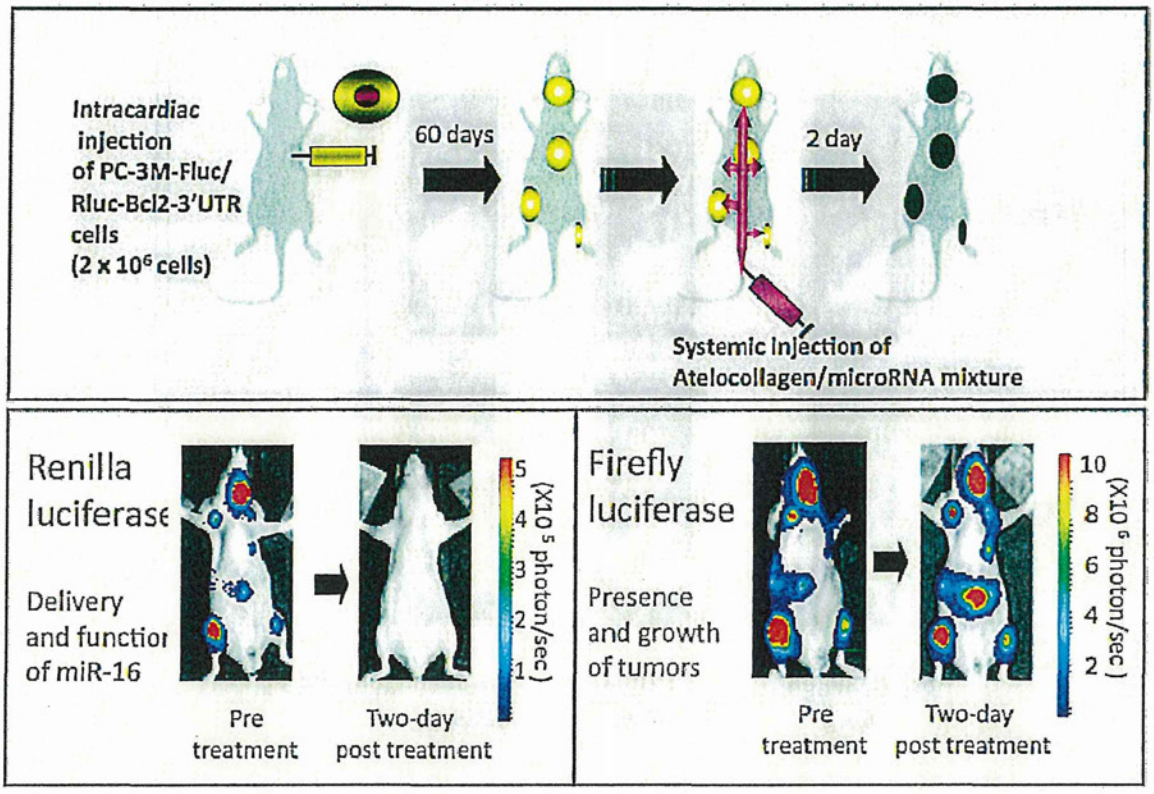

Fig. 5. Dual luciferase cells (PC-3M-Fluc/Rluc-Bcl2-3'UTR) were injected into the heart of mice and formed bone metastases. When the expression of Renilla luciferase from tumor cells could be detected, 50 μg miR-16/atelocollagen was injected intravenously. As can be seen at the bottom of the figure (left side), the photons from the Renilla luciferase were dramatically suppressed one day post-treatment. This result indicates that atelocollagen has the potential for delivering miR-16 throughout the whole body, including bone metastatic sites. Firefly luciferase was not affected, because large-sized tumors like these were not inhibited by a single treatment of miR-16 (29).

4. Notes

1. Avoid mixing by vortexing; otherwise, large aggregates may generate and cause a less efficient delivery of the oligonucleotides.
2. After mixing, ensure there are no visible aggregates.
3. Draw the mixture slowly to avoid incorporation of bubbles.
4. Intratumoral injection is also possible for delivery of atelocollagen/siRNA.
5. The effect of siRNA, such as miRNA delivery by atelocollagen, differs depending on the oligonucleotide sequence, expression level of the target oligonucleotides, the difference in target tumor cells, tissues, site of the tumors, etc. Investigating the

most suitable duration after administration for analysis of gene downregulation is recommended.

6. When the needle is correctly positioned into the left ventricle, bright red oxygenated blood influxes into the needle hub (**13, 24**). In this model, bone metastases developing in the jaws and/or legs of the mice are detected by non-invasive in vivo bioluminescence imaging.
7. For systemic administration of 200 μl of the mixture, taking 20–30 s will enhance delivery efficacy.
8. In drug resistant tumors, sometimes in vivo bioluminescence imaging does not work well since the luciferin substrate and oligonucleotide mixture are not easily taken up by drug-resistant tumor cells (**14**).
9. Atelocollagen is a highly purified type I collagen that is modified to have low immunogenicity (Koken, Tokyo). Atelocollagen forms nanosize particles when it is mixed with synthetic miRNAs, via electrostatic binding. The nanoparticles are easily incorporated into cells by endocytosis. The atelocollagen/oligonucleotide complex showed high resistance to nucleases. Therefore, the complex is thought to be stable in vivo (**12, 29**).
10. It is possible to prepare luciferase-expressing cells with a virus vector system. To generate lentiviral-vector particles containing the luciferase gene, an HIV-1 gag–pol expression plasmid, an HIV-1 Rev expression plasmid and a VSV-G envelope protein expression plasmid were used to package the HIV-based expression vector. In brief, four plasmids were co-transfected into 293FT cells. Two days after transfection, the supernatants were cleared from the cellular debris by low-speed centrifugation (10 min, 1,000 × *g*) and filtration through 0.45-μm filters. Aliquots were stored at −80°C.

Acknowledgements

This work was supported in part by a Grant-in-Aid for the Third-Term Comprehensive 10-Year Strategy for Cancer Control, a Grant-in-Aid for Scientific Research on Priority Areas Cancer from the Ministry of Education, Culture, Sports, Science and Technology, and the Program for Promotion of Fundamental Studies in Health Sciences of the National Institute of Biomedical Innovation (NiBio), and a Takeda Science Foundation.

References

1. Bass, B.L. (2000) Double-stranded RNA as a template for gene silencing. *Cell* **101**, 235–238.
2. Mcmanus, M.T. and Sharp, P.A. (2003) Gene silencing in mammals by small interfering RNAs. *Nat Rev Genet* **3**, 737–747.
3. Shankar, P., Manjunath, N., and Lieberman, J. (2005) The prospect of silencing disease using RNA interference. *JAMA* **293**, 1367–1373.
4. Leung, R.K., Whittaker, P.A. (2005) RNA interference: from gene silencing to gene-specific therapeutics. *Pharmacol Ther* **107**, 222–239.
5. Behlke, M.A. (2006) Progress towards in vivo use of siRNAs. *Mol Ther* **13**, 644–670.
6. Dykxhoorn, D.M., Palliser, D., and Lieberman, J. (2006) The silent treatment: siRNAs as small molecule drugs. *Gene Ther* **13**, 541–552.
7. Rayburn, E.R., Wang, H., and Zhang, R. (2006) Antisense-based cancer therapeutics: are we there yet? *Expert Opin Emerg Drugs* **11**, 337–352.
8. Hagan, J.P. and Croce, C.M. (2007) MicroRNAs in carcinogenesis. *Cytogenet Genome Res* **118**, 252–259.
9. Jiang, J., Gusev, Y., Aderca, I., Mettler, T.A., Nagorney, D.M., Brackett, D.J., Roberts, L.R., and Schmittgen, T.D. (2008) Association of microRNA expression in hepatocellular carcinomas with hepatitis infection, cirrhosis, and patient survival. *Clin Cancer Res* **14**, 419–427
10. Bartel, D.P. (2004) MicroRNAs: genomics, biogenesis, mechanism, and function. *Cell* **116**, 281–297.
11. Osaki, M., Takeshita, F., and Ochiya, T. (2008) MicroRNA as biomarkers and therapeutic drugs in human cancer. *Biomarkers* **13**, 658–670.
12. Minakuchi, Y., Takeshita, F., Kosaka, N., Sasaki, H., Yamamoto, Y., Kouno, M., Honma, K., Nagahara, S., Hanai, K., Sano, A., Kato, T., Terada, M., and Ochiya, T. (2004) Atelocollagen-mediated synthetic small interfering RNA delivery for effective gene silencing in vitro and in vivo. *Nucleic Acids Res* **32**:e109.
13. Takeshita, F., Minakuchi, Y., Nagahara, S., Honma, K., Sasaki, H., Hirai, K., Teratani, T., Namatame, N., Yamamoto, Y., Hanai, K., Kato, T., Sano, A., and Ochiya, T. (2005) Efficient delivery of small interfering RNA to bone-metastatic tumors by using atelocollagen in vivo. *Proc Natl Acad Sci USA* **102**, 12177–12182.
14. Honma, K., Iwao-Koizumi, K., Takeshita, F., Yamamoto, Y., Yoshida, T., Nishio, K., Nagahara, S., Kato, K., and Ochiya, T. (2008) *RPN2* gene confers docetaxel resistance in breast cancer. *Nat Med* **14**, 939–948.
15. Takei, Y., Kadomatsu, K., Goto, T., and Muramatsu, T. (2006) Combinational antitumor effect of siRNA against midkine and paclitaxel on growth of human prostate cancer xenografts. *Cancer*, **107**, 864–873.
16. Vooijs, M., Jonkers, J., Lyons, S., and Berns, A. (2002) *Cancer Res* **62**, 1862–1867.
17. Hoffman, R.M. (1999) Orthotopic transplant mouse models with green fluorescent protein-expressing cancer cells to visualize metastasis and angiogenesis. *Cancer and Metastasis Reviews* **17**, 271–277.
18. Hoffman, R.M. (1999) Orthotopic metastatic mouse models for anticancer drug discovery and evaluation: a bridge to the clinic. *Invest New Drugs* **17**, 343–359.
19. Hoffman, R.M. (2002) In vivo imaging of metastatic cancer with fluorescent proteins. *Cell Death Differ* **9**, 786–789.
20. Hoffman, R.M. (2005) Orthotopic metastatic (MetaMouse) models for discovery and development of novel chemotherapy. *Methods Mol Med* **111**, 297–322.
21. Nakanishi, H., Ito, S., Mochizuki, Y., and Tatematsu, M. (2005) Evaluation of chemosensitivity of micrometastases with green fluorescent protein gene-tagged tumor models in mice. *Methods Mol Med* **111**, 351–362.
22. Hennig, R., Ventura, J., Segersverd, R., Ward, E., Ding, X.Z., Rao, S.M., Jovanovic, B.D., Iwamura, T., Talamonti, M.S., Bell, R.H. Jr, and Adrian, T.E. (2005) LY293111 improves efficacy of gemcitabine therapy on pancreatic cancer in a fluorescent orthotopic model in athymic mice. *Neoplasia* **7**, 417–425.
23. Contag, P.R., Olomu, I.N., Stevenson, D.K., and Contag, C.H. (1998) Bioluminescent indicators in living mammals. *Nat Med* **4**, 245–247.
24. Rehemtulla, A., Stegman, L.D., Cardozo, S.J., Gupta, S., Hall, D.E., Contag, C.H., and Ross, B.D. (2000) Rapid and quantitative assessment of cancer treatment response using in vivo bioluminescence imaging. *Neoplasia* **2**, 491–495.
25. Jenkins, DE, Oei, Y, Hornig, YS, Yu, S.F., Dusich, J., Purchio, T., and Contag, P.R. (2003) Bioluminescent imaging (BLI) to improve and refine traditional murine models of tumor growth and metastasis. Clin Exp Metastasis **20**, 733–744.